Meccanica (2011) 46:1023–1033
DOI 10.1007/s11012-010-9358-0

Entropy generation due to natural convection in a partially heated cavity by local RBF-DQ method

Soheil Soleimani · A. Qajarjazi · H. Bararnia · A. Barari · G. Domairry

Received: 22 November 2009 / Accepted: 13 September 2010 / Published online: 15 October 2010

Abstract The Local Radial Basis Function-Differential Quadrature (RBF-DQ) method is applied to two-dimensional incompressible Navier-Stokes equations in primitive form. Numerical results of heatlines and entropy generation due to heat transfer and fluid friction have been obtained for laminar natural convection. The variations of the entropy generation for different Rayleigh numbers are also investigated. Comparison between the present results and previous works demonstrated excellent agreements which verify the accuracy and flexibility of the method in simulating the fluid mechanics and heat transfer problems.

Keywords Entropy generation · Heatlines · Radial basis function · Mesh-free method · Natural convection · Cavity

Nomenclature

Be	Bejan number
c	Shape parameter
$\bar{c}$	Constant in the transformed form of MQ test functions
g	Acceleration due to gravity ($\mathrm{m\,s^{-2}}$)
H	Length (m)
K	Thermal conductivity ($\mathrm{W\,m^{-1}\,K^{-1}}$)
Nu	Nusselt number
P	Dimensionless pressure
Pr	Prandtl number
p	Pressure (Pa)
Ra	Rayleigh number
S	Dimensionless entropy generation
T	Temperature (K)
T_0	Bulk temperature $(T_h + T_c)/2$ (K)
t	Time (s)
U, V	Dimensionless fluid velocities
u, v	Velocity components in x and y directions ($\mathrm{m\,s^{-1}}$)
X, Y	Dimensionless Cartesian coordinates
x, y	Cartesian coordinates (m)

Greek symbols

α	Thermal diffusivity ($\mathrm{m^2\,s^{-1}}$)
β	Volumetric coefficient of thermal expansion ($\mathrm{K^{-1}}$)
μ	Viscosity ($\mathrm{N\,s\,m^{-2}}$)
ν	Kinematic viscosity ($\mathrm{m^2\,s^{-1}}$)
ρ	Fluid density ($\mathrm{kg\,m^{-3}}$)
τ	Dimensionless time
ϕ	Irreversibility distribution ratio

S. Soleimani · A. Qajarjazi · H. Bararnia · G. Domairry
Mechanical Engineering Faculty, Babol University of Technology, Babol, Iran

A. Barari (✉)
Department of Civil Engineering, Aalborg University, Sohngårdsholmsvej 57, 9000 Aalborg, Denmark
e-mail: amin78404@yahoo.com

A. Barari
e-mail: ab@civil.aau.dk

Subscripts

c	Cold
f	Fluid
$f.f$	Fluid friction
h	Hot
$h.t$	Heat transfer
l	Local
t	Total

1 Introduction

Traditional numerical techniques such as finite difference and finite volume methods are routinely used to solve complex problems and they require significant effort in mesh generation. Mesh-free methods, on the other hand, have generated considerable interest due to the ability to overcome the high cost of mesh generation [1–5]. Recently, another group of mesh-free methods, based on the radial basis functions (RBFs), have become attractive for solving partial differential equation (PDEs). Kansa [6, 7] introduced the direct collocation method using RBFs. It is found that RBFs are able to construct an interpolation scheme with favorable properties such as high efficiency, good quality and capability of dealing with scattered data, especially for higher dimension problems. The truly mesh-free nature of RBFs motivated researchers to use them to deal with partial differential equations. To approximate derivatives by RBFs, Shu and his co-workers [8–10] proposed the RBF-DQ method. This method combines the differential quadrature (DQ) approximation [11–14] of derivatives and function approximation of RBF. Previous applications showed that RBF-DQ is an efficient method to solve linear and nonlinear PDEs [15, 16]. Generally, the local RBF-DQ method is very flexible and simple in code writing and it can be easily applied to linear and nonlinear problems. In the local form of RBF-DQ method the problem of ill-conditioned global matrix has been removed by replacement of global solvers by block partitioning schemes for large simulation problems as shown in Fig. 1.

On the other hand, simulation of natural convection in rectangular enclosures has received considerable attention in the recent years [17–19] due to its vast applications in mechanical engineering. Besides, numerous works on entropy generation, relating to natural and forced convection [20–25] demonstrate the importance of the topic. In this study, the second law of thermodynamics has been applied to the cavity problem to determine entropy generations due to heat and flow transport for two different cases. Comparison of the present study with some previous works confirms the accuracy and applicability of the method in fluid mechanic and heat transfer.

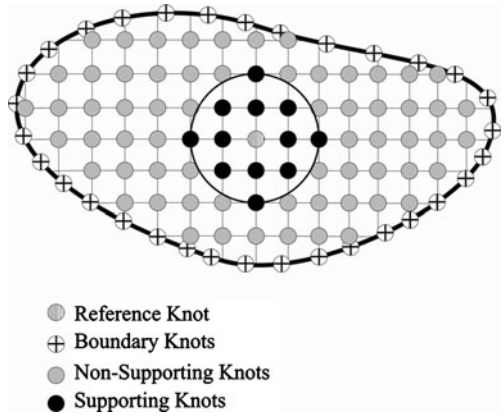

Fig. 1 Supporting knots around a centered knot

2 Local RBF-DQ method

This method is different from the conventional RBF-based collocation methods which are based on the function approximation. The RBF-DQ method directly approximates the derivatives. So, it can be easily applied to the linear and nonlinear problems.

2.1 Differential quadrature method (DQ)

The DQ method is a numerical discretization technique for approximation of derivatives which is initiated from the idea of conventional integral quadrature [12]. In this method the mth order derivative of a function $f(x)$ with respect to x at a point x_i can be approximated by DQ as

$$f_x^{(mt)}(x_i) = \sum_{j=1}^{N} w_{ij}^m f(x_j), \quad i = 1, 2, \ldots, N, \tag{1}$$

where x_j are the discrete points in the domain, $f(x_j)$ and $w_{ij}^{(m)}$ are the function values at these points and the related weighting coefficients respectively.

2.2 Local MQ-DQ method formulation

As discussed in detail by Shu et al. [8], in LMQDQ method, the MQ-RBF is used as the basic function to determine the weighting coefficients in the DQ approximation of derivatives for a two-dimensional problem. They showed that the weighting coefficient matrix $[W^n]$ can be determined by

$$[G][W^n]^T = \{G_x\}, \tag{2}$$

In which $[G]$ and $[G_x]$ are known matrices.

3 Shape parameter (c) in local MQ-DQ method

The MQ approximation of the function contains a shape parameter c that can be knot-dependent and must be determined by the user. In local MQ-DQ method, the shape parameter has a strong effect on the accuracy of the numerical results. The difficulty of assigning the different values of c, when the knots are randomly generated, can be removed by normalization of scale in the supporting region [8]. The constant in the transformed form of MQ test functions ($\bar{c}$) can be taken as 3.1, and the number of supporting knots as 16.

4 Mathematical modeling

Geometry of the problem with related boundary condition is depicted for two cases in Fig. 2. The continuity, momentum and energy equations for a two dimensional laminar flow of an incompressible Newtonian fluid are written with the following assumptions: the gravity acts in the vertical direction, fluid properties are constant and fluid density variations are neglected except in the buoyancy term (the Boussinesq approximation) and radiation heat exchange is negligible. Using non-dimensional variables, the dimensionless form of the governing equations [22] can be written as

$$\frac{\partial U}{\partial X} + \frac{\partial V}{\partial Y} = 0, \tag{3}$$

$$\frac{\partial U}{\partial \tau} + U\frac{\partial U}{\partial X} + V\frac{\partial U}{\partial Y} = -\frac{\partial P}{\partial X} + \Pr\left(\frac{\partial^2 U}{\partial X^2} + \frac{\partial^2 U}{\partial Y^2}\right), \tag{4}$$

$$\frac{\partial V}{\partial \tau} + U\frac{\partial V}{\partial X} + V\frac{\partial V}{\partial Y} = -\frac{\partial P}{\partial Y} + \Pr\left(\frac{\partial^2 V}{\partial X^2} + \frac{\partial^2 V}{\partial Y^2}\right) + \Pr \mathrm{Ra} T, \tag{5}$$

$$\frac{\partial T}{\partial \tau} + U\frac{\partial T}{\partial X} + V\frac{\partial T}{\partial Y} = \left(\frac{\partial^2 T}{\partial X^2} + \frac{\partial^2 T}{\partial Y^2}\right). \tag{6}$$

The steady-state solutions are obtained from unsteady-state equations (3)–(6). The dimensionless variables in above equations are defined as

$$(X, Y) = (x, y)/H, \qquad (U, V) = (u, v)/(\alpha/H),$$

$$P = p/\rho(\alpha/H)^2,$$

$$T = (t - t_c)/\Delta T \quad \text{and} \quad \tau = \alpha t/H^2,$$

by using $H, \alpha/H, \Delta T = t_h - t_c$ as characteristic scales for length, velocity and temperature respectively. The

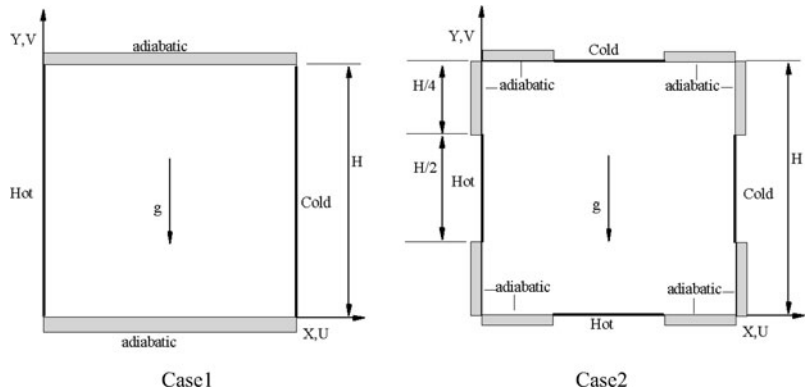

Fig. 2 Geometrical details of the cases

non-dimensional parameters, Rayleigh number and Prandtl number are defined as

$$\mathrm{Ra} = g\beta \Delta t H^3/\nu\alpha, \qquad \mathrm{Pr} = \nu/\alpha. \tag{7}$$

4.1 Boundary conditions

No-slip condition is imposed for velocities on the solid walls. Thermal boundary conditions are $T = 1$ for heat sources, $T = 0$ for sinks and $\frac{\partial T}{\partial n} = 0$ for the insulated walls.

4.2 Entropy generation

According to the dimensionless parameters and local thermodynamic equilibrium of the linear transport theory [22], the dimensionless local entropy generation due to heat transfer and fluid friction for a two-dimensional flow in Cartesian coordinates and in explicit form can be written as:

$$S_{l.h.t} = \left(\frac{\partial T}{\partial X}\right)^2 + \left(\frac{\partial T}{\partial Y}\right)^2, \tag{8}$$

$$S_{l.f.f} = \phi\left\{2\left[\left(\frac{\partial U}{\partial X}\right)^2 + \left(\frac{\partial V}{\partial Y}\right)^2\right] + \left(\frac{\partial U}{\partial Y} + \frac{\partial V}{\partial X}\right)^2\right\}. \tag{9}$$

The local entropy generation number which is called entropy generation number, is the summation of $S_{l.f.f}$ and $S_{l.h.t}$:

$$\begin{aligned} S_l &= S_{l.h.t} + S_{l.h.t} \\ &= \left(\frac{\partial T}{\partial X}\right)^2 + \left(\frac{\partial T}{\partial X}\right)^2 + \phi\left\{2\left[\left(\frac{\partial U}{\partial X}\right)^2 + \left(\frac{\partial V}{\partial Y}\right)^2\right] + \left(\frac{\partial U}{\partial Y} + \frac{\partial V}{\partial X}\right)^2\right\}. \end{aligned} \tag{10}$$

where ϕ is the irreversibility distribution ratio:

$$\phi = \frac{S_{l.f.f}}{S_{l.h.t}} = \frac{\mu T_0}{k}\left(\frac{\alpha}{H\Delta T}\right)^2. \tag{11}$$

The total entropy generation is obtained by integrating the dimensionless local entropy generation over the system volume:

$$S_{t.h.t} = \int_V S_{l.h.t}\,dV, \qquad S_{t.f.f} = \int_V S_{l.f.f}\,dV, \qquad S_t = S_{t.h.t} + S_{t.f.f}. \tag{12}$$

The local Bejan number indicates the strength of the entropy generation due to heat transfer irreversibility:

$$\mathrm{Be}_l = \frac{S_{l.h.t}}{S_l}. \tag{13}$$

For any location inside the cavity, the condition of $\mathrm{Be}_l > 1/2$ implies that the heat transfer irreversibility is dominating, while the condition $\mathrm{Be}_l < 1/2$ indicates that the fluid friction irreversibility is dominating. For $\mathrm{Be}_l = 1/2$, the heat transfer and viscous irreversibilities are equal.

4.3 Heat function and heatlines

The concept of heat function and heatlines are firstly suggested and defined by Kimura and Bejan [26] in 1983. Heatlines exhibit the convective heat transport process from a microscopic view. It is informative to note that heatlines are lines across which the net flow of energy is zero. Heatlines are expected to be parallel to adiabatic walls and normal to the isothermal wall. The heatlines are employed in the present work to visualize the heat transport processes. Heat function (θ) is defined in terms of the energy equation as

$$\frac{\partial \theta}{\partial Y} = UT - \frac{\partial T}{\partial X}, \qquad -\frac{\partial \theta}{\partial X} = VT - \frac{\partial T}{\partial Y}. \tag{14}$$

At a general knot of index i, the present local RBF-DQ approximation of (8), (9) and (14) can be written as

$$S_{l.h.t} = \left(\sum_{k=1}^{n_i} c_{i,k}^{1x} T_i^k\right)^2 + \left(\sum_{k=1}^{n_i} c_{i,k}^{1y} T_i^k\right)^2, \tag{15}$$

$$S_{l.f.f} = \phi\left\{2\left[\left(\sum_{k=1}^{n_i} c_{i,k}^{1x} U_i^k\right)^2 + \left(\sum_{k=1}^{n_i} c_{i,k}^{1y} V_i^k\right)^2\right] + \left(\sum_{k=1}^{n_i} c_{i,k}^{1y} U_i^k + \sum_{k=1}^{n_i} c_{i,k}^{1x} V_i^k\right)^2\right\}, \tag{16}$$

$$\begin{aligned} \frac{\partial \theta}{\partial Y} &= U_i T_i - \sum_{k=1}^{n_i} c_{i,k}^{1x} T_i^k, \\ -\frac{\partial \theta}{\partial X} &= V_i T_i - \sum_{k=1}^{n_i} c_{i,k}^{1y} T_i^k, \end{aligned} \tag{17}$$

where F_i represents the function value at knot i, F_i^k represents the function value at the kth supporting knot

for knot i. $c_{i,k}^{1x}, c_{i,k}^{1y}, c_{i,k}^{2x}$ and $c_{i,k}^{2y}$ represent the computed weighting coefficients in the DQ approximation for the first and second order derivatives in the x and y direction respectively.

5 Numerical procedure

The set of governing equations is numerically solved by LRBF-DQ with a two step fractional method formulation which is applied to 2D N-S equations with a collocated arrangement. The procedure is described in detail by Shan et al. [27]. For the present study, regular point distribution is used as shown in Fig. 4. The number of knots are 2601 (for $\mathrm{Ra} = 10^3$ and $\mathrm{Ra} = 10^4$) and 5625 (for $\mathrm{Ra} = 10^5$). The convergence criteria is $|\xi_{i,j}^n - \xi_{i,j}^{n-1}| < 10^{-4}$ where ξ stands for U, V and T and n denoting the iteration. The problem is solved for $\mathrm{Pr} = 0.7$.

To commence the numerical procedure, intermediate velocity U^* and V^* are predicted by advection-diffusion equation, which drops the pressure term.

$$\frac{U^* - U^n}{\Delta\tau} = -\frac{1}{2}(u^* \cdot \nabla U^* + u^n \cdot \nabla U^n) + \frac{1}{2}\mathrm{Pr}(\Delta U^* + \Delta U^n), \tag{18}$$

$$\frac{V^* - V^n}{\Delta\tau} = -\frac{1}{2}(u^* \cdot \nabla V^* + u^n \cdot \nabla V^n) + \frac{1}{2}\mathrm{Pr}(\Delta V^* + \Delta V^n) + \mathrm{Pr}\,\mathrm{Ra} T^n, \tag{19}$$

where u is the velocity vector (U, V) and the superscript n denotes the values at the current step. For the first step all those values are guessed by the user, which are usually set to zero. The complete velocity $\boldsymbol{u}$ at t^{n+1} is corrected by including the pressure field, given by

$$\frac{u^{n+1} - u^*}{\Delta\tau} = -\nabla p^{n+1}. \tag{20}$$

The final velocity field is subject to the continuity constraint given by

$$\nabla \cdot u^{n+1} = 0. \tag{21}$$

Substituting (20) into (21) leads to the following Poisson equation for pressure

$$\Delta p^{n+1} = \frac{\nabla \cdot u^*}{\Delta\tau}. \tag{22}$$

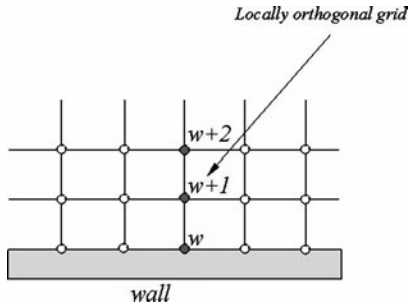

Fig. 3 Locally orthogonal grid near the boundary

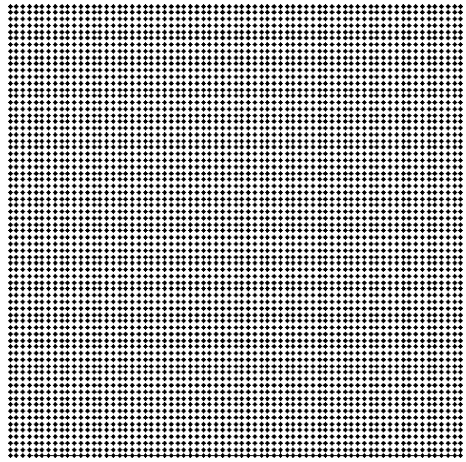

Fig. 4 Regular knots distribution for natural convection problem

The velocity u^{n+1} is updated by the solution of pressure equation (22) and (20). For the heat transfer equation we have

$$\frac{T^{n+1} - T^n}{\Delta\tau} = -U^{n+1}\frac{\partial T^n}{\partial X} - V^{n+1}\frac{\partial T^n}{\partial Y} + \left(\frac{\partial^2 T^n}{\partial X^2} + \frac{\partial^2 T^n}{\partial Y^2}\right). \tag{23}$$

The updated velocities from the previous steps are inserted to yield the updated value of T^{n+1}.

5.1 Implementation of boundary conditions

The physical boundary conditions of the problem are explained earlier. In addition to the physical boundary conditions above, some other boundary conditions are worthy of attention: The enforcement of continuity equation on the solid boundary. To achieve this, con-

tinuity equation should be accurately enforced on the solid boundary, i.e.

$$\frac{\partial(u \cdot n)}{\Delta n} = 0, \tag{24}$$

where n is the normal direction to the surface boundary. For generality and consistency, implementation of above Neumann boundary condition is carried out by using the so-called locally orthogonal "grid" [8] shown in Fig. 3 as follows

$$T_w = \frac{4T_{w+1} - T_{w+2}}{3}. \tag{25}$$

The reason of adopting this type of grid is for easy implementation. Using locally orthogonal grid, the Neumann boundary condition for the velocity components can be discretized by one-side finite difference scheme. Then, this discretized boundary condition is used to update the corresponding velocity component at immediate interior point of the boundary knot (not the boundary knot itself), since the velocity on the boundary is already known. For the adiabatic surfaces the same procedure can be applied.

It is worthwhile mentioning that although the solution procedure is carried out for a simple geometry in this work, the present procedure can be applied to complex shapes.

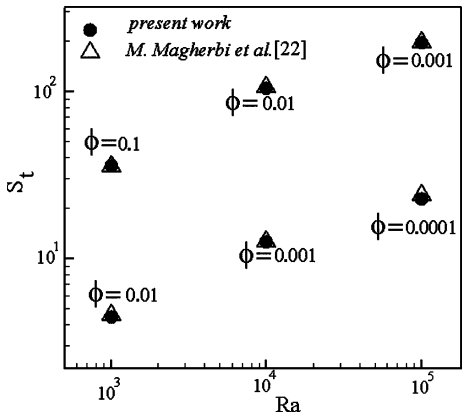

Fig. 5 Comparison of total entropy generation between present results and previous work [22] for case1

6 Results and discussion

Numerical results are presented through Figs. 5–11 to demonstrate the effects of different Rayleigh numbers

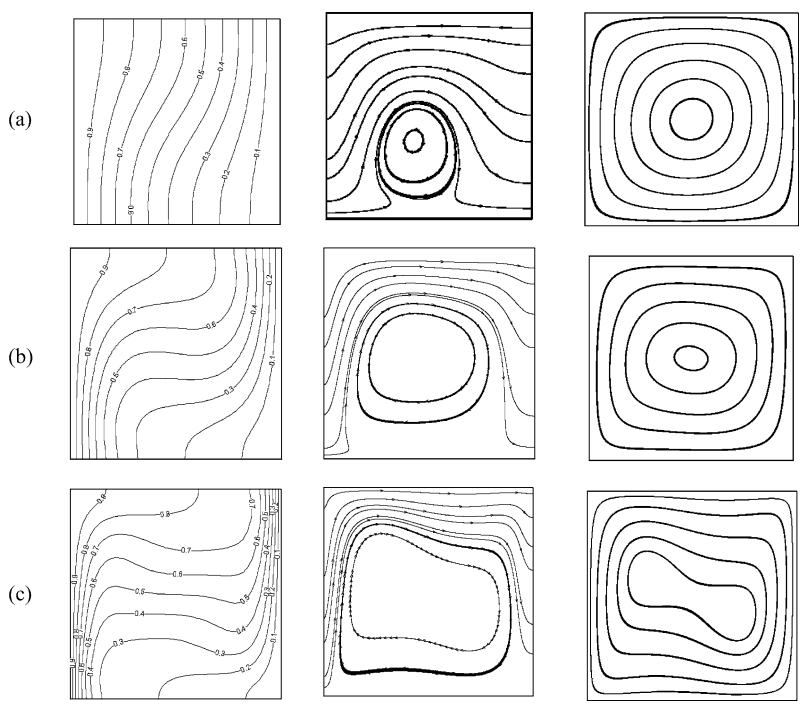

Fig. 6 (**a**) Ra $= 10^3$, (**b**) Ra $= 10^4$, (**c**) Ra $= 10^5$, the *first column*: temperature fields, the *second column*: heatlines and the *third column*: streamlines for the case1

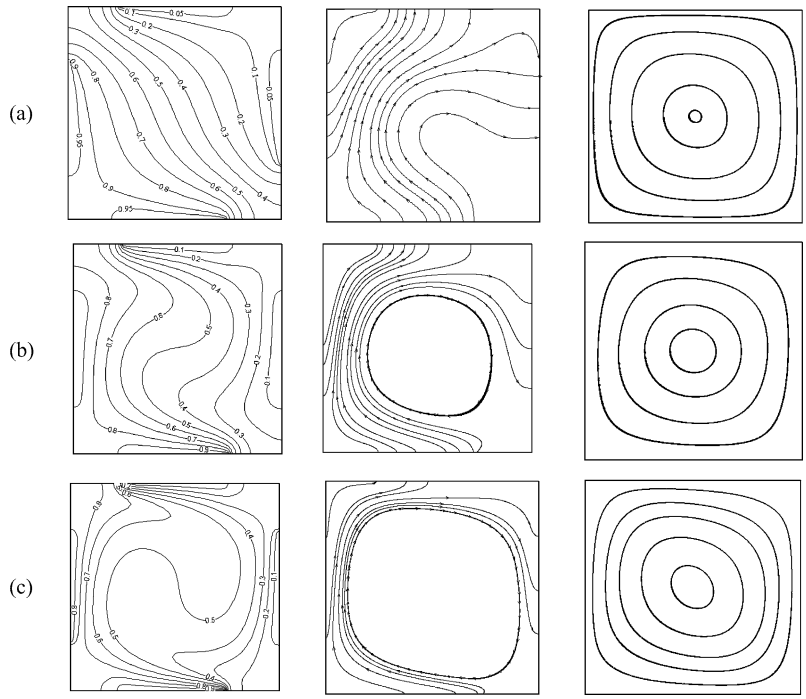

Fig. 7 (**a**) $\mathrm{Ra} = 10^3$, (**b**) $\mathrm{Ra} = 10^4$, (**c**) $\mathrm{Ra} = 10^5$, the *first column*: temperature fields, the *second column*: heatlines and the *third column*: streamlines for the case2

Table 1 Comparison between present results and previous works for case1

	$\mathrm{Ra} = 10^4$			$\mathrm{Ra} = 10^5$		
	Davis [28]	Shu [8]	Present	Davis [28]	Shu [8]	Present
$\lvert\psi_{\mathrm{mid}}\rvert$	5.071	5.084	5.077	9.11	9.146	9.097
$\psi_{\max}$	N/A	N/A	N/A	9.612	9.648	9.6061
$u_{\max}$	16.178	16.169	16.167	34.730	34.547	34.528
$v_{\max}$	19.617	19.631	19.642	68.59	69.313	67.799
Nu_0	2.238	2.24	2.241	4.509	4.573	4.536
$\mathrm{Nu}_{\max}$	3.528	3.560	3.549	7.717	7.844	7.742
$\mathrm{Nu}_{\min}$	0.586	0.584	0.584	0.729	0.726	0.729

on heatline, streamline, and entropy generation for two cases studied in this work. Also, in order to compare the performance of local RBF-DQ method, different quantities are computed and compared with the ones in previous works by Davis [26], Shu [8] and Maghrebi et al. [20]. As it is clear in Table 1, there is an excellent agreement between the results for case 1 confirming the high accuracy of the meshless method.

Figure 5 illustrates the comparison of total entropy generation between present results and the previous work [22] for case1. Figures 6, 7 show the streamlines, isotherms and heatlines for $\mathrm{Ra} = 10^3$, 10^4 and 10^5 for both cases. It is found that for both cases in low Rayleigh numbers, flow intensity is very low and heat transfer occurs mainly by conduction. As Rayleigh number increases, more deflection occurs in heatlines which implies the convective heat flow strength. For case1, for a low Rayleigh number ($\mathrm{Ra} = 10^3$) isotherms are nearly vertical, and the heatlines are nearly horizontal; as expected for a conduction dominated problem. It is also observed that heat leaves the hot wall in an almost uniform way

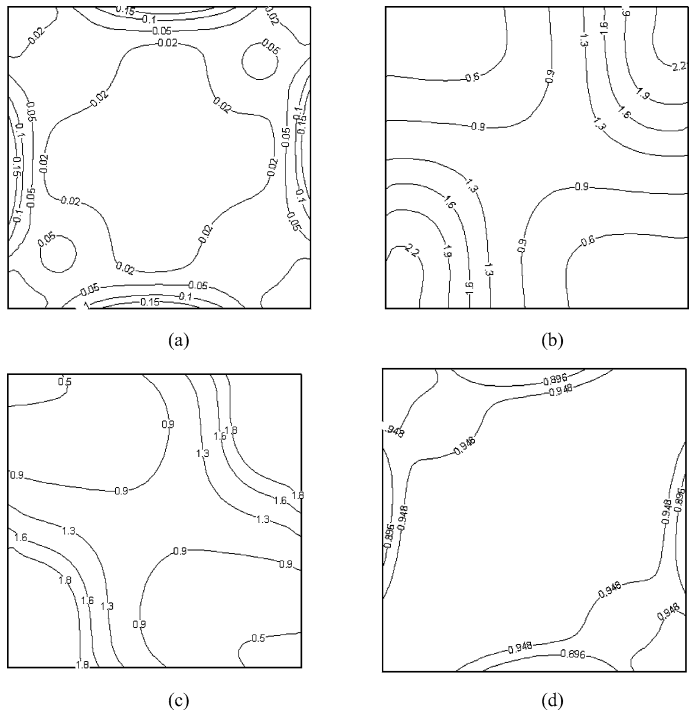

Fig. 8 (**a**) Local entropy generation due to fluid friction, (**b**) local entropy generation due to heat transfer, (**c**) local entropy generation, (**d**) local Bejan number at $\mathrm{Ra} = 10^3$ and $\phi = 10^{-4}$ for case1

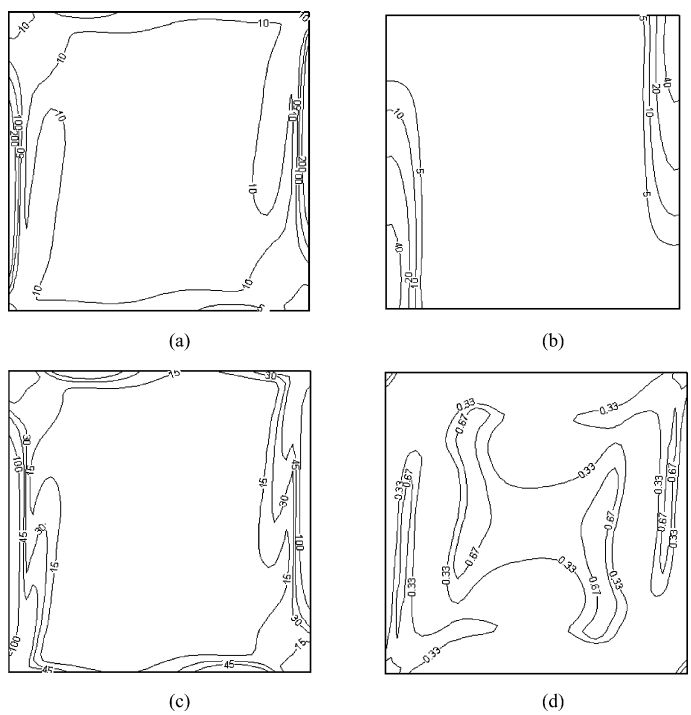

Fig. 9 (**a**) Local entropy generation due to fluid friction, (**b**) local entropy generation due to heat transfer, (**c**) local entropy generation, (**d**) local Bejan number at $\mathrm{Ra} = 10^5$ and $\phi = 10^{-4}$ for case1

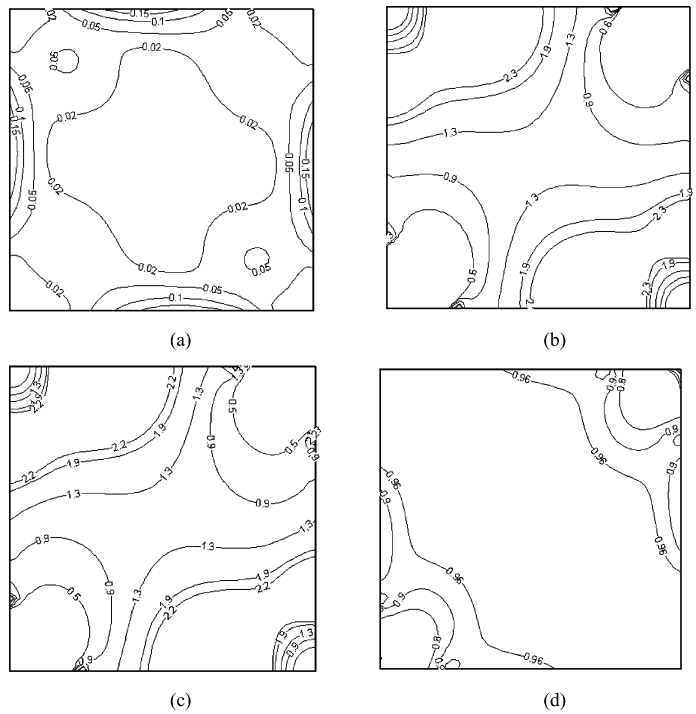

Fig. 10 (**a**) Local entropy generation due to fluid friction, (**b**) local entropy generation due to heat transfer, (**c**) local entropy generation, (**d**) local Bejan number at $\mathrm{Ra} = 10^3$ and $\phi = 10^{-4}$ for case2

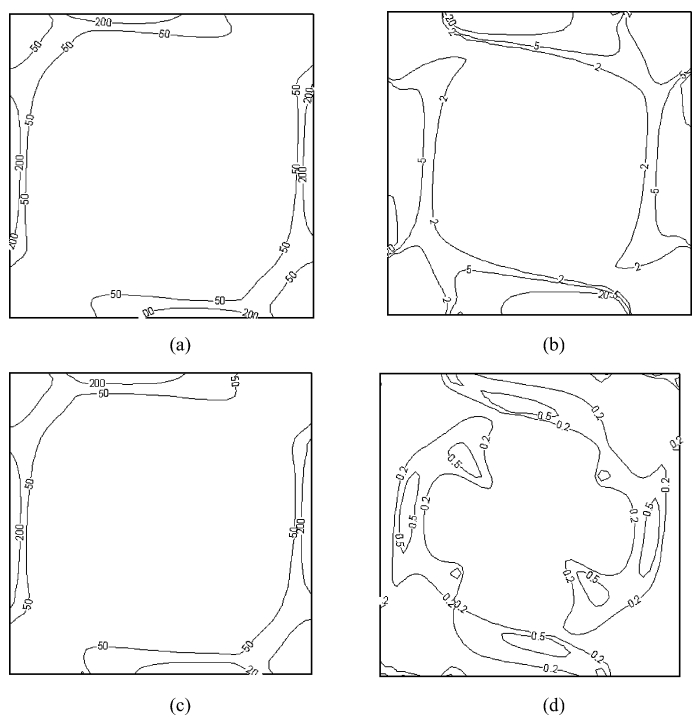

Fig. 11 (**a**) Local entropy generation due to fluid friction, (**b**) local entropy generation due to heat transfer, (**c**) local entropy generation, (**d**) local Bejan number at $\mathrm{Ra} = 10^5$ and $\phi = 10^{-4}$ for case2

and reaches the cold wall in almost the same way. However, for a high Rayleigh number, Fig. 6(c), the flow intensity is more obvious and the isotherms get far from the vertical walls that indicate the convection is dominant. For case2 (Fig. 7), the configuration of the heatlines show that the heat released by the bottom source is absorbed by both sinks and the heat picked up by the fluid from the left source is not conveyed to the sink on the right but the one on the top.

The local entropy generation due to fluid friction ($S_{l.f.f}$), heat transfer ($S_{l.h.t}$), local entropy generation (S_l) and local Bejan number (Be_l) is shown in Figs. 8–11 for different Rayleigh numbers and $\phi = 10^{-4}$ for both cases. It is clear that in low Rayleigh number (Figs. 8 and 10), the maps of local entropy generation are similar to the local entropy generation due to heat transfer, which denotes the domination of $S_{l.h.t}$. On the other hand, for high Rayleigh number (Figs. 9 and 11), the maps of local entropy generation are similar to the local entropy generation due to fluid friction, which shows the domination of $S_{l.f.f}$ in the cavity. For case1, Figs. 8(b) and 9(b) illustrate that as the Rayleigh number increases, the $S_{l.h.t}$ is confined to the top right and bottom left edges of the isothermal walls. This is mainly due to high temperature gradients confined to these locations. It is also obvious that the adiabatic walls are inactive for entropy generation in terms of heat transfer. As shown in Figs. 10(b–d). $S_{l.h.t}$ and Be_l decrease in top right and bottom left edges of the cavity because of lower temperature gradient between two sinks or two sources. However for the other corners it is vice versa. Figures 11(b) and 11(c) show that, for higher Rayleigh number, all the edges are inactive for entropy generation due to heat transfer and fluid friction.

7 Conclusions

This study dealt with the entropy generation due to natural convection heat transfer in an enclosed cavity for two different cases. The results are obtained numerically using mesh-free Local RBF-DQ method. The meshless method is applied for two dimensional Navier-Stokes equation in primitive form. The effect of different Ra numbers on the heatlines, streamlines, and the entropy generation is shown and discussed through table and graphs. Comparison of the present results with previous works demonstrates that the Local RBF-DQ method is an attractive approach in terms of accuracy, capability and flexibility.

References

1. Nayroles B, Touzot G, Villon P (1992) Generalizing the finite element method: diffuse approximation and diffuse elements. Comput Mech 10:307–318
2. Belytschko T, Lu YY, Gu L (1994) Element-free Galerkin methods. Int J Numer Methods Eng 37:229–256
3. Liu W, Jun S, Zhang Y (1995) Reproducing kernel particle methods. Int J Numer Methods Fluids 20:1081–1106
4. Atluri SN, Zhu T (1998) New meshless local Petrov–Galerkin (MLPG) approach in computational mechanics. Comput Mech 22:117–127
5. Hildebrand G (2009) Fracture analysis using an enriched meshless method. Meccanica 44:535–545
6. Kansa EJ (1990) Multiquadrics—A scattered data approximation scheme with applications to computational fluid dynamics—I. Surface approximations and partial derivative estimates. Comput Math Appl 19:127–145
7. Kansa EJ (1990) Multiquadrics—A scattered data approximation scheme with applications to computational fluiddynamics—II. Solutions to parabolic, hyperbolic, and elliptic partial differential equations. Comput Math Appl 19:147–161
8. Shu C, Ding H, Yeo KS (2003) Local radial basis function-based differential quadrature method and its application to solve two dimensional incompressible Navier–Stokes equations. Comput Methods Appl Mech Eng 192:941–954
9. Ding H, Shu C, Tang DB (2005) Error estimates of local multiquadric-based differential quadrature (LMQDQ) method through numerical experiments. Int J Numer Methods Eng 63:1513–1529
10. Shu C, Ding H, Chen HQ, Wang TG (2005) An upwind local RBF-DQ method for simulation of inviscid compressible flows. Comput Methods Appl Mech Eng 194:2001–2017
11. Bellman RE, Kashef BG, Casti J (1972) Differential quadrature: a technique for the rapid solution of nonlinear partial differential equations. J Comput Phys 10:40–52
12. Shu C, Richards BE (1992) Application of generalized differential quadrature to solve two-dimension incompressible Navier–Stokes equations. Int J Numer Methods Fluids 15:791–798
13. Shu C, Wee KHA (2002) Numerical simulation of natural convection in a square cavity by SIMPLE-generalized differential quadrature method. Comput Fluids 31:209–226
14. Tezer-Sezgin M (2004) Solution of magnetohydrodynamic flow in a rectangular duct by differential quadrature method. Comput Fluids 33:533–547
15. Soheil S, Jalaal M, Bararnia H, Ghasemi E, Ganji DD, Mohammadi F (2010) Local RBF-DQ method for two-dimensional heat conduction problems. Int Commun Heat Mass Transf. doi:10.1016/j.icheatmasstransfer.2010.06.033

16. Bararnia H, Jalaal M, Ghasemi E, Soheil S., Ganji DD, Mohammadi F (2010) Numerical simulation of Joule heating phenomenon using meshless RBF-DQ method. Int J Thermal Sci. doi:10.1016/j.ijthermalsci.2010.06.008
17. Nithyadevi N, Sivasankaran S, Kandaswamy P (2007) Buoyancy-driven convection of water near its density maximum with time periodic partially active vertical walls. Meccanica 42:503–510
18. Saravanan S, Kandaswamy P (2002) Buoyancy convection in low Prandtl number liquids with large temperature variation. Meccanica 37:599–608
19. Ece MC, Elif B (2007) Natural convection flow under a magnetic field in an inclinedsquare enclosure differentially heated on adjacent walls. Meccanica 42:435–449
20. Zahmatkesh I (2008) On the importance of thermal boundary conditions in heat transfer and entropy generation for natural convection inside a porous enclosure. Int J Thermal Sci 47:339–346
21. Abu-Hijleh BAK, Abu-Qudais M, Abu-Nada E (1999) Numerical prediction of entropy generation due to natural convection from a horizontal cylinder. Energy 24:327–333
22. Magherbi M, Abbassi H, Brahim AB (2003) Entropy generation at the onset of natural convection. Int J Heat Mass Transf 46:3441–3450
23. Abu-Hijleh BAK, Heilen WN (1999) Entropy generation due to laminar natural convection over a heated rotating cylinder. Int J Heat Mass Transf 42:4225–4233
24. Mahmud S, Island AKS (2003) Laminar free convection and entropy generation inside an inclined wavy enclose. Int J Thermal Sci 42:1003–1012
25. Famouri M, Hooman K (2008) Entropy generation for natural convection by heated partitions in a cavity. Int Commun Heat Mass Transf 35:492–502
26. Kimura S, Bejan A (1983) The heatline visualization of convective heat transfer. ASME J Heat Transf 105:916–919
27. Shan YY, Shu C, Lu ZL (2008) Application of local MQ-DQ method to solve 3D incompressible viscous flows with curved boundary. CMES Comput Model Eng Sci 25:99–113
28. de Vahl Davis G (1983) Natural convection of air in a square cavity: a benchmark numerical solution. Int J Numer Methods Fluids 3:249–264